Preprint Title	ALD-Grown Ultrathin Coatings on Bismuth Oxyhalide Photocatalysts: The Effect of UV-ozone Pretreatment on Coating Quality
Authors	Nitai Arbell, Shakked Regev and Yaron Paz
Publication Date	29 Aug. 2023
Article Type	Full Research Paper
Supporting Information File 1	Supplementary - 1.docx; 12.0 MB
ORCID® iDs	Yaron Paz - https://orcid.org/0000-0002-8161-1123

ALD-Grown Ultrathin Coatings on Bismuth Oxyhalide Photocatalysts: The Effect of UV-ozone Pretreatment on Coating Quality

Nitai Arbell[1,2], Shakked Regev[1,2], Yaron Paz*[1,2]

Address: [1]The Russell Berrie Nanotechnology Institute, Technion-Israel Institute of Technology, Haifa 3200003, Israel [2]The Wolfson Department of Chemical Engineering, Technion-Israel Institute of Technology

Email: Paz@technion.ac.il

*Corresponding author

Keywords

ALD; Bismuth oxyhalide; UV-ozone; surface treatment

Abstract

The growth of ultrathin layers of oxides by Atomic Layer Deposition (ALD) is well documented for oxide substrates such as SiO_2, Bi_2O_3, Al_2O_3, in which oxygen is the only negatively charged atom in the substrate. In contrast, the knowledge regarding ALD growth on oxide substrates that contain other negatively charged atoms, such as halogens, is quite limited. The commonly used bismuth oxyhalide family of materials are characterized by a low density of surface hydroxyls, required for the initiation of

thermal ALD growth of oxides, thus hampering the ability to grow ultrathin layers of oxides on their surface. This restriction becomes even more severe if the process has to be performed at low temperatures. In this work, we show that low-temperature Al_2O_3 can be grown on bismuth oxyhalide materials by ALD. The coating conformality is monitored by the ability of the ultrathin layers to suppress the photocatalytic activity of the substrates. It was found that UV-ozone treatment under a humid atmosphere prior to deposition resulted in significant conformality improvement of the coatings on all catalysts.

Introduction

In recent years, atomic layer deposition (ALD) has found increasing interest and utilisation in various fields and applications, with the basic aim of growing highly controllable and conformal thin-films on a wide range of substrate types and morphologies. Its high precision in fabricating nanometric thin-films even on high-aspect ratio surfaces has given rise to its use in a variety of industries [1,2]. For example, ALD is becoming more and more important in the manufacturing of semiconductor devices, where it is used to grow highly precise, nanometric oxides, such as gate dielectrics in MOSFETs [3,4]. ALD films are also applied in the energy sector, for example as anti-corrosion barriers or protective coatings in batteries [5,6]. These layers are also utilised in the field of catalysis [7,8] and photocatalysis, where they are used as photocatalyst films [9], protective coatings [10,11], or activity-lowering dielectric coatings [12,13]. The aforementioned benefits have also made ALD a valuable method in the synthesis of polymer-based hybrid materials [14,15], as well as in incorporating organic molecules into inorganic structures, as functional moieties [16,17] or as molecular templates [18,19]. These processes require, by their nature,

mild conditions and low deposition temperatures, in order to avoid the degradation of the organic components. While low-temperature ALD processes exist for a limited arsenal of compounds [20,21], generalisation is still a challenge due to difficulties pertaining to the ALD parameters window.

Despite the steadily increasing importance and utilisation of ALD processes in both research and industry, one extremely important aspect is typically not accounted for – the effect of the substrate itself on the resulting films [22,23]. The ideal ALD growth mechanism is based on the Langmuirian adsorption of precursors on the surface of the substrate, and hence highly dependent on the available active groups on the surface, such as surface hydroxyls in the growth of metal oxides [24–27]. Deviations from chemical adsorption result in non-isotropic, non-self-limited growth, leading to non-conformal films [26,28]. There is also a strong effect of the substrate on the deposited layer's properties, such as structure and mechanical strength. This is of particular importance in the ultrathin-layer regime, where interfacial effects are still dominant, and at low deposition temperatures, where chemical bonding to the surface may be hindered. As a result, most mechanistic studies on ALD focus on "simple", well studied substrates, such as Si, SiO_2, metal oxides or metals [23,29,30]. Some work has been done towards understanding the interplay between ALD and organic polymers, but for them, and for many other families of materials, there are still a lot of uncharted territories [31,32].

With contemporary research in material science expanding into more precise applications, we have found the interplay between ALD and different substrate materials worthy of investigating. In particular, the photocatalytic BiOX family (bismuth oxyhalide, with X representing Cl, Br or I, and occasionally F), presents an interesting challenge, with the use of these materials gaining significant traction in the past decade [33,34]. These materials have excellent photocatalytic activity, part of which relies on

a direct charge-transfer mechanism, which differs from the "classical" photocatalytic mechanisms (for example in TiO_2), which are based on a surface-hydroxyl mediated mechanism [35–37]. Materials belonging to the BiOX family are easy to synthesise in a variety of morphologies and with well-defined crystal facets [38,39]. Their structure and surface properties are wildly different from traditional ALD substrates, such as oxides and metals, and they do not necessarily display surface hydroxyls, which are typically used as "docking points" for oxide ALD reactions [25,26]. Several methods have been used in an attempt to increase hydroxyl coverage, such as synthesising crystals which primarily expose hydroxylated facets [40,41], or grafting of organic molecules [42]. These approaches may be suitable for some applications, but might not be appropriate when a conformal ALD coverage of the whole exposed surface is desired, or when grafted surface organic moieties are undesired.

In this work, we have studied the effect of surface activation through UV-Ozone cleaning (UVOC), known to promote hydrophilicity by increasing hydroxyl density, [43–46], similar to the effect of plasma in direct bonding [47]. In addition, the effect of deposition temperature was tested, trying to assess the interplay between the ALD window of the precursors and the substrate surface chemistry, which is affected by this temperature as well, through changes in hydroxyl coverage [48–51]. The choice of an optimal temperature is crucial for attaining the best growth conditions for a desired application, as well as for protecting any organic compounds that may be incorporated into the structure.

The work described in this manuscript revolves around the growth of ultra-thin layers of Al_2O_3 onto BiOX substrates. The ALD efficiency and layer conformality were assessed using kinetic measurements of the photocatalytic degradation of stearic acid, as well as through physicochemical characterisation of the resulting films. It is believed

that these findings can be used for choosing the right combination of substrate and ALD processing conditions, en-route for improving ALD-based devices.

Results and Discussion

Figure 1A1 presents SEM micrographs taken from a substrate made of a film of BiOCl particles in a silica binder, coated with alumina by 10 ALD cycles, using trimethylaluminum as reactant 1 and water as reactant 2. Here, Figure 1A1 shows a sample in which the ALD process was performed without a UVOC pre-treatment, whereas Figure 1A2 depicts a sample that was subjected to UVOC pre-treatment prior to growing the first ALD layer. Figures 1B-1E display the EDS maps of O, Al, Bi, Cl, respectively, corresponding to the samples prepared without and with UVOC pre-treatment. As shown in the insets of Figure 1, the various types of atoms are more or less evenly distributed in the samples. No difference is observed between the sample that was subjected to pre-treatment and the sample that was prepared without pre-treatment. This observation was general for all types of BiOX substrates, regardless of ALD-growth temperature (see supporting information S1-S10). Likewise, micrographs taken from films prepared on substrates comprising of only BiOX, coated with alumina by ALD, showed an even distribution of Al (S11-S13).

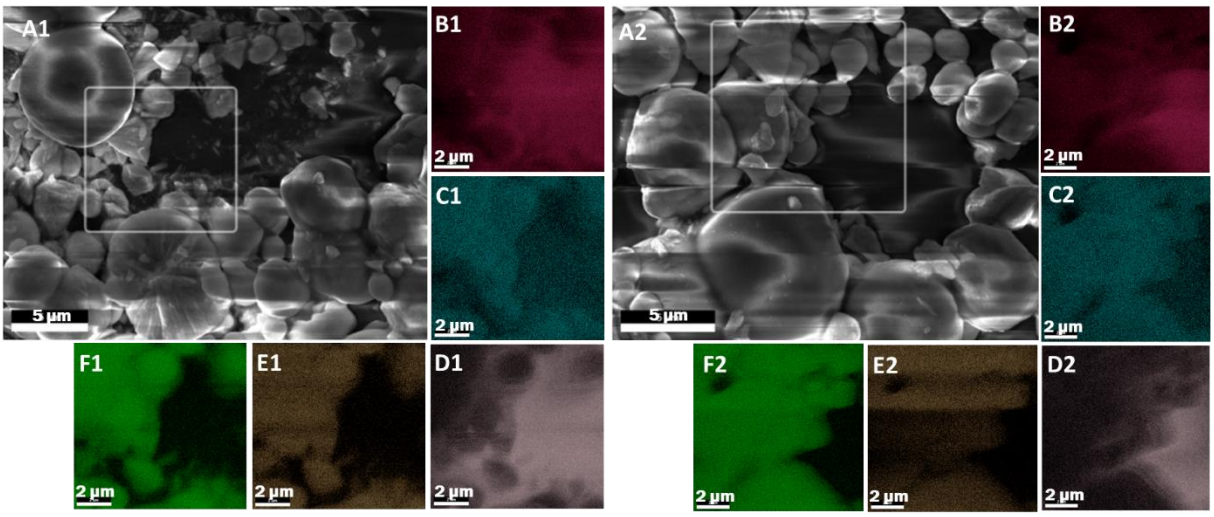

Figure 1: SEM micrograph (A) and EDS elemental maps (B-F) of the highlighted area for BiOCl in an SiO2 binder coated with 10 cycles of Al2O3 ALD at 80ºC without (A1-F1) and with (A2-F2) UV-ozone treatment. EDS legend: O (B), Al (C), Si (D), Bi (E) and Cl (F) atoms.

The averaged atomic concentrations of the various atoms, deduced from XPS measurements of similar films, i.e. 10 ALD cycles of alumina, grown at 60ºC with and without UVOC pre-treatment, are shown in Table 1. As seen in the Table, in all BiOX types, the atomic concentration of aluminium in films prepared with a pre-treatment step was very similar to that of films prepared without this step, and ranged between 11.3% to 14.4%. The ratio between bismuth and halogen atoms was in all cases higher than expected (1.16 in BiOBr to 1.74 in BiOI); the reason is not clear to us, but could be related to surface structuring or to some systematic error in the XPS sensitivity factor. The atomic concentration of oxygen (62.6% to 70.7%) was higher than expected from combining the stoichiometry of alumina and BiOX (approximately 32%), most likely due to water adsorbed on the alumina surface.

High-resolution XPS analysis of the peaks (Figures S14-S18) showed no significant shift between the different samples, suggesting that any effect incurred by the UVOC pre-treatment becomes un-noticeable due to the large contribution of Al-O bonds in the top portion of the film.

Table 1: XPS atomic concentration (%) of bismuth, aluminium, oxygen, and the relevant halide (Cl, Br or I) as measured by XPS for 10 cycle ALD coatings grown at 60ºC with (+) and without (-) UVOC pre-treatment, shown on a carbon-free basis.

Atomic %	**BiOCl**		**BiOBr**		**BiOI**	
	(+)UVOC	(-)UVOC	(+)UVOC	(-)UVOC	(+)UVOC	(-)UVOC
Bi	13.7±0.2	14.1±0.3	12.5±0.7	14.2±0.2	9.2	9.5
Al	13.8±0.1	11.7±0.3	11.9±0.0	11.3±0.2	14.3	14.4
O	63.4±0.4	65.4±0.4	64.7±1.1	62.6±0.2	70.7	68.4
X(=Cl,Br,I)	9.1±0.0	8.8±0.2	10.8±0.4	12.2±0.2	5.3	7.8

As shown above, both XPS and SEM-EDS were silent with respect to the quality of the first alumina layer, attached to the BiOX substrates. In contrast, it is possible to use mass transport, coupled with the photocatalytic property of these materials, as a tool to study the characteristics of the first ALD layers. Indeed, the photocatalytic activity of TiO_2, overcoated with ultrathin layers of silica, was found to be strongly affected by the number of atomic layers of silica [52]. For our case, the conformality of the overlaying inert alumina films is expected to correlate with lower photocatalytic activity, since pinhole defects are likely to enable mass transport of organics to the photocatalytic surface (and of oxygenating species from the photocatalyst to adsorbed organics [53]. Figure 2A presents changes in the IR spectrum of a stearic acid (SA) film deposited on an alumina-coated BiOBr substrate, following exposure to UV light. As shown in the figure the photocatalytic degradation is manifested by a decrease in all SA-related peaks. Accordingly, by plotting the intensity of the peaks it is possible to deduce the kinetics of degradation, found to be of an apparent zero order rate law (Figure 2B). Such a rate law is quite common for the photocatalytic degradation of a multilayer of stearic acid [54].

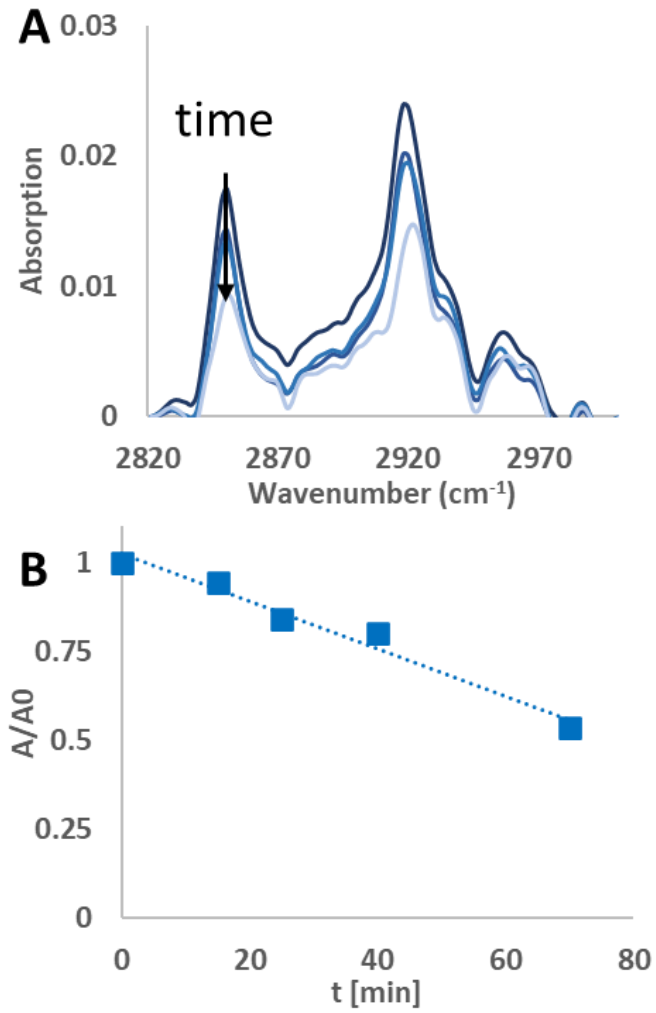

Figure 2: A – FTIR spectra of stearic acid degradation over a BiOCl substrate coated with Al_2O_3 ALD following UVOC pre-treatment, and B –fitting of the results to a zero-order rate law.

Any study of the effect of ALD growth parameters of alumina on activity damping of the underlying photocatalyst should take into account the fact that the photocatalytic activity of the substrates varies among the different types of photocatalysts. Figure 3A presents the measured zero-order rate constant for the various BiOX photocatalysts, as well as that of TiO_2, used as a benchmark which contains high density of hydroxyls

on its surface. These values were used to normalize the rate constants of the ALD-coated samples, as depicted in Figures 3B-3F. It should be noted that all measurements were performed on optically-thick samples, such that all impinging photons are absorbed. For each photocatalyst, activity was measured both for samples prepared with a UVOC pre-treatment and for samples prepared without pre-treatment. Three ALD temperatures were examined: 40°C, 60°C and 80°C, all of which can be considered as low process temperatures, which are adequate for growth of organic-inorganic hybrid devices.

As expected, for all cases, the normalized rate was lower than one, demonstrating activity damping by the alumina overlayer. A comparison of the average damping, over all conditions, between the various types of photocatalysts (Figure 3B), reveals that the activity damping in titania was considerably more pronounced than that of the three types of BiOX photocatalysts. This difference can be explained by a more compact alumina layer, relatively free of pinhole defects, formed by virtue of the high density of hydroxyls on the TiO_2 surface during the growth of the first layer.

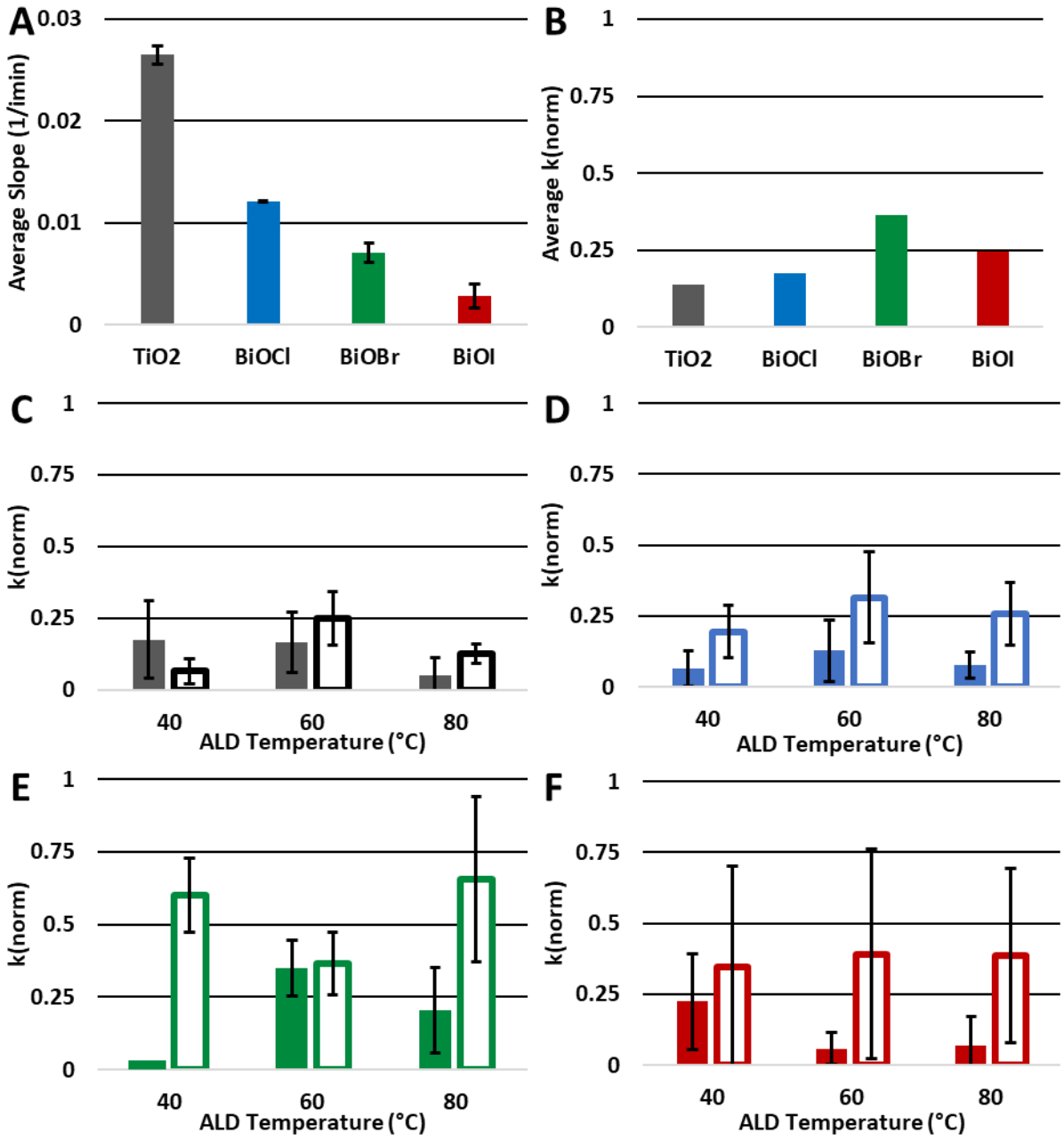

Figure 3: A – The average slopes for the photodegradation of stearic acid as calculated for each of the photocatalysts tested without ALD overcoating. B – the average normalised slope (the average slope the coated samples normalised to the value of the slope without ALD coating) for type of photocatalyst, without accounting for coating parameters C – the average slope for ALD coated TiO_2, D - the average slope for ALD coated BiOCl, E - the average slope for ALD coated BiOBr, and F- the

average slope for ALD coated BiOI. In C-F, full bars represent samples that underwent UVOC pre-treatment, and empty bars samples that did not undergo pre-treatment, with ALD performed at 40°C, 60°C, and 80°C.

The results portrayed in Figures 3C-3F clearly show that performing the UVOC pre-treatment led to higher damping of the photocatalytic activity, thus indicating an improvement in the conformality of the ALD film. The only exception was a TiO_2 substrate, coated at 40°C. The ratios between the kinetic constants of samples prepared with a UVOC pre-treatment to those of samples prepared without pre-treatment are given in Figure 4. Averaging over all preparation temperatures and BiOX types, the introduction of a UVOC pre-treatment step yields films whose average activity was approximately 3 times lower. For TiO_2, this effect was somewhat muted, reflecting the notion that (at least at low temperature) there was no need for increasing the density of surface hydroxyls. No clear effect of the preparation temperature on the beneficial effect of UVOC pre-treatment was found. This may indicate, alas not prove, the presence of hidden parameters having contradictory influence.

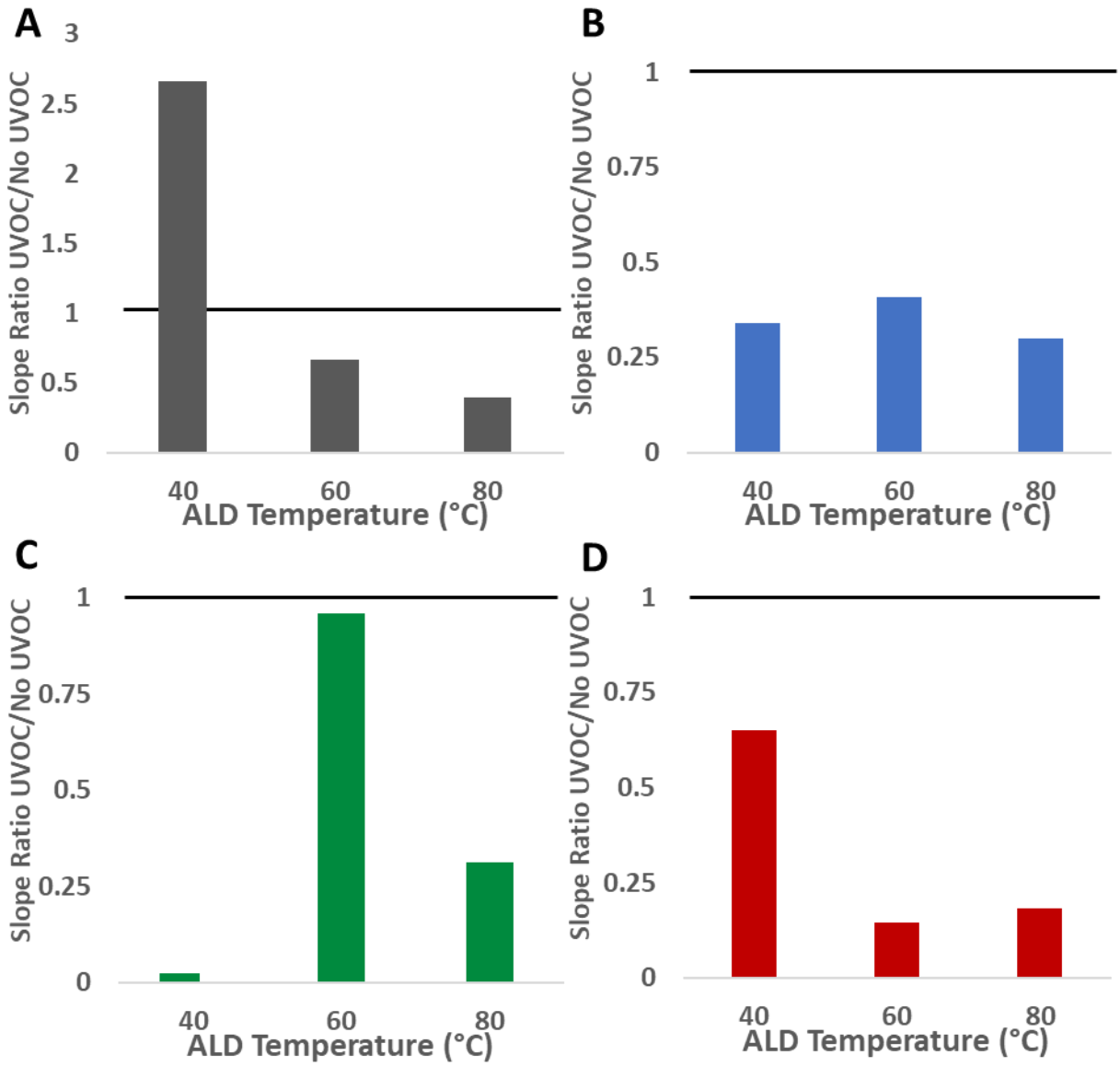

Figure 4: the UVOC-dependent ratio of the activity damping parameter (the slope value with UVOC pre-treatment over the value without) after ALD coating, performed at 40°C, 60°C and 80°C, for A – TiO_2, B – BiOCl, C – BiOBr and D - BiOI.

The effect of the UVOC pre-treatment on the growth of alumina by ALD is illustrated in Figure 5. In the absence of pre-treatment (Figure 5A), the anchoring of the aluminium atoms in the first layer is inadequate, leading to incomplete coverage. Successive layers partially bridge-over these voids, reaching aluminium density that approaches

that of a well- packed layer, as appeared in our EDS-SEM and XPS measurements. Still, the underlying pores, and the less rigid structure enable mass transport through the layer manifested by fast photocatalytic degradation. The introduction of a UV-ozone cleaning of the surface, under humid conditions increases the density of anchoring points on the surface, makes the first layer to be highly conformal and well-packed. Consequently, mass transport through the layer is hampered, leading to damped degradation kinetics of the stearic acid (Figure 5B).

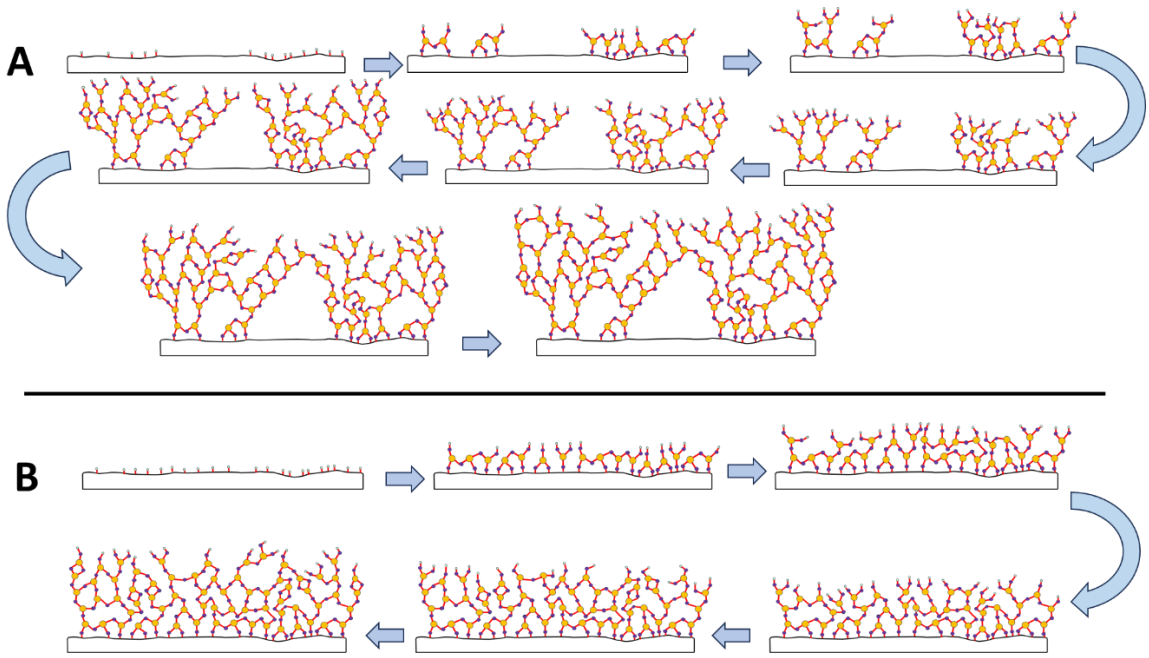

Figure 5: Illustration of layer-by-layer growth of alumina on BiOX substrates in the absence (A) and following UVOC pre-treatment (B). For clarity, and due to the reduced dimensionality of the illustration, the coordination numbers of aluminium and oxygen were set to 3 and 2, respectively, instead of 6 and 4.

Conclusion

This research shows, for the first time to our knowledge, the ALD growth of aluminium oxide on bismuth oxyhalides and, in particular, at low temperatures (40-80°C). The deposition performed here was in the ultrathin regime (10 ALD cycles), where substrate effects are most apparent. SEM and XPS were found to be silent with respect to the quality and conformality of such layers. Nevertheless, using photocatalysis as a tool for investigation of mass transport through the overcoating inert layer revealed that exposing the surface of the substrate to UV-ozone environment under humid conditions has a significant beneficial effect on the quality of the grown layers. This finding paves the way for the development of oxide ALD layers on oxide substrates that contain non-oxygen negatively charged atoms, such as halogens. Moreover, the capability to form dense, conformal oxide layers on these substrates at low temperature opens a door to the preparation of hybrid organic-inorganic devices on BiOX compounds.

Experimental

Photocatalytic films were deposited on Si wafers cut into 1''x0.5'' (for investigation of the effect of temperature on the coating) or 0.5''x0.5'' (for investigation of the effect of UVOC treatment) pieces, cleaned with ethanol, acetone and twice with deionised water, followed by immersion in aqua regia for an hour, another deionized water wash, drying overnight at 60ºC, and finally, UVOC treatment (Jelight Company, Inc.) for 10 minutes under humid conditions (a water reservoir inside the cleaning chamber).

BiOX (X=Cl, Br, I) films were grown according to a protocol adapted from Shen et al. [55], with some changes applied. A 2 M aqueous solution of the relevant acid halide

was prepared, with Bi_2NO_3 stirred in to make a 387.5 mg/ml solution. Ethylene glycol and triethanolamine were added at 2.7 and 4.2 %v/v respectively. After stirring overnight, the suspensions were sonicated for 45 min and left to settle. 25% of the total volume (2 ml for an originally 8 ml solution) was removed from the resulting clear supernatant liquid, with another 1/3 of the original volume (2.66 ml for an originally 8 ml solution) added instead as isopropyl alcohol. The films were comprised of two consecutive layers, applied via spin coating (Setcas LLC) at 3000 RPM, with overnight drying at 60ºC following deposition of each layer.

TiO_2 films were also grown as a reference, according to published sol-gel process [56]. Here, three (for the temperature effect test) or two (for the UVOC effect) layers were deposited by spin-coating at 1500 RPM, with intermittent calcination.

Part of these films were then UVOC-treated for 10 min with a water vessel in the chamber to increase surface hydrophilation, All the films apart from the controls were then sent for overcoating with Al_2O_3 by thermal ALD using a Fiji G2 system (Veeco Instruments Inc.), with trimethylaluminium (TMA) and H_2O as precursor and oxidiser respectively, and argon as the carrier gas. The full procedure was as follows: introducing the films into the reaction chamber, pumping down to base pressure (0.148 torr) and heating of the sample stage to the desired temperature overnight, followed by activating of the surface with two 0.12 sec pulses of TMA at 80 sccm carrier gas flowrate. Next, 10 cycles of alternately pulsed TMA and H_2O were applied. For growth at 40ºC and 60ºC the pulse lengths were 0.1 sec, separated by 12 sec of argon purging, whereas for growth at 80ºC, pulse lengths of 0.15 sec, separated by purging for 15 sec were used.

XPS analysis was performed using a Versaprobe III system (Physical Electronics Inc.), using a Focused X-Ray AlKα monochromated X-rays source, operating at 200 micrometres beam size, 50 W, and 15 kV. EDS and SEM analyses were performed

using a Helios NanoLab DualBeam G3 UC system (FEI Company) operating at 25 kV. XRD analysis was performed using a MiniFlex II system (Rigaku Corporation).

The photocatalytic kinetics were investigated according to a previously described method using the apparent 0-order degradation of stearic acid, monitored via a Vertex 70v FTIR (Bruker Ltd.) [52,56,57]. Samples were placed in parallel under a wide-band, 365 nm centred UV fluorescent lamp, at a uniform distance of 14.5 cm, with measurements taken after specific exposure times.

Supporting Information

The supporting information file contains further EDS mappings of ALD-coated bismuth oxyhalide films, and high resolution XPS analyses of bismuth oxyhalide films coated with or without surface pre-treatment

Acknowledgements

The authors would like to thank Dr. Kamira Weinfeld, Mrs. Valentina Korchnoy, Miss Lital Felzenshtein for their help with the technical aspects of this project. Additional thanks are given to the Russell-Berrie Nanotechnology Institute for using their facilities and for their financial support.

References

(1) George, S. M. *Chem Rev* **2010**, *110*, 111-131.

(2) Cremers, V.; Puurunen, R. L.; Dendooven, J. *Applied Physics Reviews* **2019**, *6*, No. 021302.

(3) Chen, K. Y.; Yang, C. C.; Huang, C. Y.; Su, Y. K. *RSC Adv* **2020**, *10*, 9902-9906.

(4) Shih, H. Y.; Chu, F. C.; Das, A.; Lee, C. Y.; Chen, M. J.; Lin, R. M. *Nanoscale Res Lett* **2016**, *11*, No. 235.

(5) Liu, J.; Sun, X. *Nanotechnology* **2015**, *26*, No. 024001.

(6) Cao, Y.; Meng, X.; Li, A. *Energy and Environmental Materials* **2021**, *4*, 363-391.

(7) Wang, X.; Zhao, Z.; Zhang, C.; Li, Q.; Liang, X. *Catalysts*, **2020**, *10*, No. 1298.

(8) Oneill, B. J.; Jackson, D. H. K.; Lee, J.; Canlas, C.; Stair, P. C.; Marshall, C. L.; Elam, J. W.; Kuech, T. F.; Dumesic, J. A.; Huber, G. W. *ACS Catal* **2015**, *5*, 1804–1825.

(9) Eswar, N. K. R.; Singh, S. A.; Heo, J. *J. Mater. Chem. A* **2019**, *7*, 17703-17734.

(10) Krýsová, H.; Neumann-Spallart, M.; Tarábková, H.; Janda, P.; Kavan, L.; Krýsa, J. *Beilstein Journal of Nanotechnology* **2021**, *12, 24-34*.

(11) Liu, D.; Liu, Y.; Candelaria, S. L.; Cao, G.; Liu, J.; Jeong, Y.-H. *Journal of Vacuum Science & Technology A* **2012**, *30*, No. 01A123.

(12) Pham, K.; Pelisset, S.; Kinnunen, N.; Karvinen, P.; Hakala, T. K.; Saarinen, J. J. *Mater Chem Phys* **2022**, *277*, No. 125533.

(13) Guo, J.; van Bui, H.; Valdesueiro, D.; Yuan, S.; Liang, B.; van Ommen, J. R. *Nanomaterials* **2018**, *8*, No. 61.

(14) Petit, R. R.; Li, J.; van de Voorde, B.; van Vlierberghe, S.; Smet, P. F.; Detavernier, C. *ACS Appl Mater Interfaces* **2021**, *13*, 46151–46163.

(15) Zhang, Z.; Simon, A.; Abetz, C.; Held, M.; Höhme, A. L.; Schneider, E. S.; Segal-Peretz, T.; Abetz, V. *Advanced Materials* **2021**, *33*, No. 2105251.

(16) Edri, E.; Frei, H. *Journal of Physical Chemistry C* **2015**, *119*, 28326–28334.

(17) Lin, C.; Tsai, F. Y.; Lee, M. H.; Lee, C. H.; Tien, T. C.; Wang, L. P.; Tsai, S. Y. *J Mater Chem* **2009**, *19*, 2999-3003.

(18) Arbell, N.; Bauer, K.; Paz, Y. *ACS Appl Mater Interfaces* **2021**, *13*, 39781–39790.

(19) Canlas, C. P.; Lu, J.; Ray, N. A.; Grosso-Giordano, N. A.; Lee, S.; Elam, J. W.; Winans, R. E.; van Duyne, R. P.; Stair, P. C.; Notestein, J. M. *Nat Chem* **2012**, *4*, 1030–1036.

(20) Neubieser, R. M.; Wree, J. L.; Jagosz, J.; Becher, M.; Ostendorf, A.; Devi, A.; Bock, C.; Michel, M.; Grabmaier, A. *Micro and Nano Engineering* **2022**, *15*, No. 100126.

(21) Ansari, M. Z.; Nandi, D. K.; Janicek, P.; Ansari, S. A.; Ramesh, R.; Cheon, T.; Shong, B.; Kim, S. H. *ACS Appl Mater Interfaces* **2019**, *11*, 43608–43621.

(22) Schmitt, P.; Beladiya, V.; Felde, N.; Paul, P.; Otto, F.; Fritz, T.; Tünnermann, A.; Szeghalmi, A. v. *Coatings* **2021**, *11*, No. 173.

(23) Tiurin, O.; Ein-Eli, Y. *Advanced Materials Interfaces* **2019**, *6*, No. 1901455.

(24) Richey, N. E.; de Paula, C.; Bent, S. F. *J. Chem. Phys.* **2020**, *152*, No. 040902.

(25) Puurunen, R. L. *J Appl Phys* **2004**, *95*, 4777-4786.

(26) Lemaire, P. C.; King, M.; Parsons, G. N. *J. Chem. Phys.* **2017**, *146*, No. 052811.

(27) Wind, R. A.; George, S. M. *J Phys Chem A* **2010**, *114*, 1281-1289.

(28) Zhang, W.; Engstrom, J. R. *Journal of Vacuum Science & Technology A* **2016**, *34*, No. 01A107.

(29) Bilousov, O. v.; Voznyi, A.; Landeke-Wilsmark, B.; Villamayor, M. M. S.; Nyberg, T.; Hägglund, C. *Chem. Mater.* **2021**, *33*, 2901–2912.

(30) Ding, J. N.; Wang, X. F.; Yuan, N. Y.; Li, C. L.; Zhu, Y. Y.; Kan, B. *Surf Coat Technol* **2011**, *205*, 2846-2851.

(31) Parsons, G. N.; Atanasov, S. E.; Dandley, E. C.; Devine, C. K.; Gong, B.; Jur, J. S.; Lee, K.; Oldham, C. J.; Peng, Q.; Spagnola, J. C.; Williams, P. S. *Coordination Chemistry Reviews* **2013**, *257*, 3323–3331.

(32) Keskiväli, L.; Heikkilä, P.; Kenttä, E.; Virtanen, T.; Rautkoski, H.; Pasanen, A.; Vähä- nissi, M.; Putkonen, M. *Coatings* **2021**, *11*, No. 1028.

(33) An, H.; Du, Y.; Wang, T.; Wang, C.; Hao, W.; Zhang, J. *Rare Metals* **2008**, *27*, 243-250.

(34) Yang, Y.; Zhang, C.; Lai, C.; Zeng, G.; Huang, D.; Cheng, M.; Wang, J.; Chen, F.; Zhou, C.; Xiong, W. *Advances in Colloid and Interface Science* **2018**, *254*, 76-93.

(35) Garg, S.; Yadav, M.; Chandra, A.; Sapra, S.; Gahlawat, S.; Ingole, P. P.; Pap, Z.; Hernadi, K. *RSC Adv* **2018**, *8*, 29022-29030.

(36) Náfrádi, M.; Hernadi, K.; Kónya, Z.; Alapi, T. *Chemosphere* **2021**, *280*, 130636.

(37) Tryba, B.; Toyoda, M.; Morawski, A. W.; Nonaka, R.; Inagaki, M. *Appl Catal B* **2007**, *71*, 163-168.

(38) Ye, L.; Su, Y.; Jin, X.; Xie, H.; Zhang, C. *Environmental Science: Nano* **2014**, *1*, 90-112.

(39) Benisti, I.; Paz, Y. *J Electrochem Soc* **2019**, *166*, No. H3257.

(40) Wang, X.; Zhang, Y.; Zhou, C.; Huo, D.; Zhang, R.; Wang, L. *Appl Catal B* **2020**, *268*, No. 118390.

(41) Zhan, G.; Li, J.; Hu, Y.; Zhao, S.; Cao, S.; Jia, F.; Zhang, L. *Environ Sci Nano* **2020**, *7*, 1454-1463.

(42) Du, C.; Nie, S.; Feng, W.; Zhang, J.; Qi, M.; Liang, Y.; Wu, Y.; Feng, J.; Dong, S.; Liu, H.; Sun, J. *Chemosphere* **2022**, *287*, No. 132246.

(43) Hobart, K. D.; Colinge, C. A.; Ayele, G.; Kub, F. J. UV/Ozone Activation Treatment for Wafer Bonding. In *Proceedings - Electrochemical Society*; 2003; Vol. 19, pp 137.

(44) Le-The, H.; Tiggelaar, R. M.; Berenschot, E.; van den Berg, A.; Tas, N.; Eijkel, J. C. T. *ACS Nano* **2019**, *13*, 6782–6789.

(45) Lü, H. F.; Yan, W. P.; Liu, Z. H.; Li, J. C. *Guang Pu Xue Yu Guang Pu Fen Xi/Spectroscopy and Spectral Analysis* **2016**, *36*, 1033-1037.

(46) Delplanque, A.; Henry, E.; Lautru, J.; Leh, H.; Buckle, M.; Nogues, C. *Appl Surf Sci* **2014**, *314*, 280-285.

(47) Pasternak, L.; Paz, Y. *RSC Adv* **2018**, *8*, 2161-2172.

(48) Groner, M. D.; Fabreguette, F. H.; Elam, J. W.; George, S. M. *Chemistry of Materials* **2004**, *16*, 639-645.

(49) Iqbal, J.; Jilani, A.; Ziaul Hassan, P. M.; Rafique, S.; Jafer, R.; Alghamdi, A. A. *J King Saud Univ Sci* **2016**, *28*, 347-354.

(50) Volp, G.; Grassian, V. H. *Chemical Communications* **2013**, *49*, 3071-3094.

(51) Brady, P. v. *Geochim Cosmochim Acta* **1992**, *56*, 2941-2946.

(52) Nussbaum, M.; Paz, Y. *Physical Chemistry Chemical Physics* **2012**, *14*, 3392-3399.

(53) Haick, H.; Paz, Y. *J. Phys. Chem. B* **2001**, *105*, 3045–3051.

(54) Paz, Y.; Heller, A.; Introduction, I. *J Mater Res* **1997**, *12*, 2759 – 2766.

(55) Shen, F.; Zhou, L.; Shi, J.; Xing, M.; Zhang, J. *RSC Adv* **2015**, *5*, 4918-4925.

(56) Paz, Y.; Luo, Z.; Rabenberg, L.; Heller, A. *J Mater Res* **1995**, *10*, 2842–2848.

(57) Smirnova, N.; Fesenko, T.; Zhukovsky, M.; Goworek, J.; Eremenko, A. *Nanoscale Res Lett* **2015**, *10*, No. 500.